A Cobalt(II)-containing Metal-Organic Framework Showing Catalytic Activity in Oxidation Reactions

Ying Lu[a], Markus Tonigold[a], Björn Bredenkötter[a], Dirk Volkmer[a,*], Julia Hitzbleck[b], and Gerhard Langstein[b]

[a] Ulm/Germany, Ulm University, Institute of Inorganic Chemistry II, Materials and Catalysis
[b] Leverkusen/Germany, Bayer MaterialScience AG, BMS-CD-NB-NT

Dedicated to Professor Bernt Krebs on the Occasion of his 70th Birthday

Abstract. A metal-organic framework (MOF) containing redox active Co^{II} atoms, $[Co^{II}(BPB)]\cdot 3DMF$ **(1)**, has been prepared from the solvothermal reaction of Co^{II} nitrate and 1,4-bis(4′-pyrazolyl)benzene (H_2-BPB) in dimethylformamide (DMF). Compound **1** constitutes a porous coordination framework that is built up by interconnecting 1D Co^{II} polymer chains with $(BPB)^{2-}$ ligands. The thermal stability of **1** was investigated by thermogravimetric (TG) analysis and variable-temperature X-ray powder diffraction (VTXRPD), which indicate that the framework of **1** is stable upon removal of solvent molecules. The argon adsorption isotherm of **1** at 77 K indicates a porous structure with a BET surface area of 1207 m^2/g. As a test reaction for catalytic activity of **1**, the oxidation of cyclohexene was examined employing tert-butyl hydroperoxide as oxidant. The maximum substrate conversion achieved after 12 h was 62 % with an estimated turn-over number (TON) of 44 based on the number of converted substrate molecules (cyclohexene) per Co^{II} atom.

Introduction

Porous materials are attracting the attention of chemists and material scientists due to commercial interest in their applications in gas storage, chemical separations and heterogeneous catalysis [1]. During the past decade, the field of porous materials has grown fast and a demand for a host of applications has developed [2]. Although a huge range of structurally diverse porous materials are reported in the literature including patents, the rational design and functionalization of porous materials tailored for a specific application is still a great challenge. Metal-organic frameworks (MOFs) show several advantages if compared to other porous materials, which result from the more flexible design of structural building units and the straight-forward post-synthetic functionalization of inner pore surfaces [3], which, along with other features such as high micropore volumes, large surface areas and a high volume fraction of active metal sites, render MOFs very interesting heterogeneous catalysts for driving reactions at low temperature (typically << 200 °C). The promise of using MOFs in advanced catalytic applications therefore has led very recently to first investigations on catalytic applications [4].

We have recently initiated a research program focusing on MOFs containing redox-active cobalt atoms [5]. Our incentives for these investigations came from the fact that several low-molecular Co^{II} complexes have been reported previously as efficient oxygenation catalysts for alkane and alkene oxidations [6]. In these metal complexes divalent cobalt ions, situated in a four- or five-fold coordination environment, retain free coordination sites that are readily accessible for oxidants giving rise to catalytically active trivalent cobalt atoms. The prototypic catalytic reactions of these molecular Co^{II} catalysts have led to many efforts of introducing tetrahedral Co^{II} ions into microporous alumino (or gallo-) phosphates and zinco-phosphates [7]. So far, however, limited efforts have been devoted to prepare MOFs that contain accessible redox-active Co^{II} atoms [8].

Concerning the preparation of Co^{II} containing MOFs, our general synthetic strategy is to identify appropriate low-dimensional Co^{II} coordination compounds from literature and to interconnect these with suitable organic linkers. The synthesis of compound **1** reported here, is based on the fundamental structure of infinite one-dimensional chains consisting of tetrahedrally coordinated Co^{II} sites that are bridged by pyrazolate moieties, which has been previously reported by *Masciocchi* and co-workers [9]. Replacing the simple bidentate pyrazole ligand in the compound $[Co(pz)_2]$ with a back-to-back bonded linear bis-pyrazole ligand, therefore, should lead to formation of a 3D MOF. In order to obtain such Co^{II} based framework, we prepared the

* Professor Dr. Dirk Volkmer
Ulm University, Institute of Inorganic Chemistry II, Materials and Catalysis
Albert-Einstein-Allee 11
D-89081 Ulm/Germany
Fax: (+)49 (0)731 50-23039
E-mail: dirk.volkmer@uni-ulm.de

ligand 1,4-bis(4′-pyrazolyl)benzene (H_2-BPB) (Scheme 1) [10]. Reacting H_2-BPB with a suitable Co^{II} precursor under solvothermal conditions leads to the formation of the novel MOF $[Co^{II}(BPB)]\cdot 3DMF$ **(1)**, which possesses a porous framework built via 1D cobalt coordination chains interconnected with $(BPB)^{2-}$ ligands.

Experimental Section

Materials and methods

Tert-butyl hydroperoxide (70 % H_2O solution) was dried over anhydrous $MgSO_4$. Tert-butyl-2-cyclohexenyl-1-peroxide was synthesized according to a literature procedure [11]. Other materials were obtained from commercial suppliers and used without further purification. Fourier transform infrared (FT-IR) spectra were recorded from KBr pellets in the range of 4000−400 cm^{-1} on a Bruker IFS FT-IR spectrometer. Elemental analyses (C, H, N) were carried out on a Perkin-Elmer 2400 Elemental Analyzer. Melting points (uncorrected) were recorded on a Büchi Melting Point B-540 apparatus. Thermogravimetric analysis (TGA) was performed with a TGA/SDTA851 Mettler Toledo analyzer in a temperature range from 30 to 800 °C in flowing oxygen at a heating rate of 10 °C/min. Variable-temperature X-ray powder diffraction (VTXRPD) patterns were measured using a PANalytical X'Pert PRO diffractometer with an Anton Paar HTK 1200N high temperature device ($\theta-\theta$ mode, Cu Kα radiation, λ = 1.5406 Å) under static air. Powder diffraction patterns were collected over the angular range 2θ = 5−50° with a step size of 0.03°. UV/Vis diffuse reflectance spectra (DRS) were recorded on an Analytik Jena Specord 50 UV/Vis spectrometer in the range of 190−1100 nm. Argon gas sorption isotherms were measured with a Quantachrome Autosorb-I ASI-CP-8 instrument. Prior to sorption measurements, samples of chloroform-exchanged **1** were heated at 150 °C for 30 h in high-vacuum to remove included solvent molecules. Argon sorption experiments were performed at 77 K in the range of $1.00 \times 10^{-5} \leq P/P_0 \leq 1.00$ with argon. Pore size distributions were calculated using Non-Local Density Functional Theory (NLDFT) with a carbon equilibrium transition kernel for argon adsorption at 77 K, based on a slit-pore model as implemented in version 1.27 of the ASWin software package included in the Autosorb-1 system (Quantachrome Instruments, Boynton Beach, Florida USA). NMR spectra were recorded by using a Bruker Avance 400 spectrometer. Chemical shifts are given in ppm with spectra referenced to the residual solvent peak. CI mass spectra were recorded by using a Finnigan MAT, SSQ 7000 mass spectrometer equipped with a single-stage-quadrupole system. Intensities are given relative to the base peak. Gas chromatographic analyses were carried out with a Carlo Erba GC 8380 gas chromatographic instrument with a hydrogen flame ionization detector. GC-MS data were recorded on a Varian GC 3800-Varian Saturn 2000 MS instrument equipped with a WLD/ECD detector and a Chrompack column (CP-5842, 25 m long).

Synthesis of 1,4-Bis(4′-pyrazolyl)benzene (H_2-BPB)

A solution of 1,4-phenylenediacetic acid (3.88 g, 20 mmol) in 10 mL of DMF was added dropwise to the Vilsmeier-complex, prepared by adding phosphorous oxychloride (11 mL, 0.12 mol) at 0 °C to DMF (11.4 mL, 0.15 mol). The resulting mixture was stirred at 70 °C for 18 h, then cooled to r.t. and poured onto crushed ice (100 g), made basic with saturated aq. NaOH after which it was filtered. The filtrate was concentrated, the resulting solid was refluxed with 100 mL ethanol for 10 min and insoluble byproducts were removed by hot filtration. 5 mL hydrazine hydrate (0.1 mol) was added to the filtrate and the resulting mixture was refluxed for 3 h. After cooling to r.t., the product was collected by filtration, washed with ethanol and dried in vacuum to give 1.8 g (8.6 mmol, 43 %) H_2-BPB as a pale yellow solid. No melting point, decomposition at 290 °C. ^{1}H NMR (400 MHz, DMSO-d_6, 25 °C, ppm): δ 12.92 (s_{br}, 2H, NH), 8.09 (s, 4H, Hpz−H), 7.62 (s, 4H, PhH) (Figure S5, Supplementary Part); ^{13}C NMR (100 MHz, DMSO-d_6, 25 °C, ppm): δ 131.43, 126.43, 121.99 (Figure S6, Supplementary Part). Elemental analysis calcd. for $C_{12}H_{10}N_4$ (%): C, 68.56; N, 26.65; H, 4.79; Found: C, 67.72; N, 26.19; H, 4.91. MS (CI): m/z (%): 239 (23) $[M+C_2H_5]^+$, 211 (100) $[M+H]^+$.

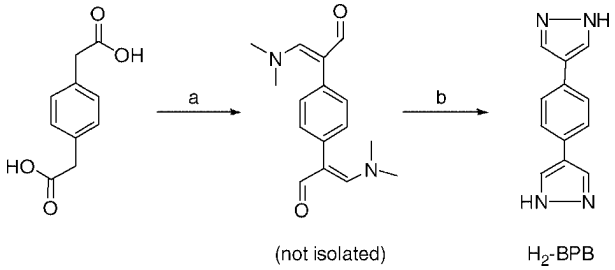

Scheme 1 Synthesis of the ligand H_2-BPB: a) Vilsmeier-complex, DMF, 70 °C, 18 h; b) hydrazine hydrate, EtOH, reflux, 3 h.

Synthesis of 1

H_2-BPB (8 mg, 38 μmol) and $Co(NO_3)_2\cdot 6H_2O$ (40 mg, 137 μmol) were dissolved in 4 mL DMF. 0.02 mL 1 M aq. HCl was added and the resulting solution was placed in a heating tube. The tube was sealed and heated (0.2 °C/min) to 120 °C for 3 days to yield 11.1 mg **1** (60 % based on H_2-BPB) as purple crystals. Elemental analysis calcd. for $C_{21}H_{29}CoN_7O_3$ (**1**) (%): C, 51.80; H, 5.96; N, 20.14; found: C, 50.41; H, 5.57; N, 19.60. IR (KBr, cm^{-1}): 3436(br), 3336(br), 2925(w), 2853(w), 2329(w), 1672(s), 1576(m), 1490(w), 1435(m), 1384(s), 1351(m), 1251(s), 1176(m), 1123(m), 1090(m), 1052(s), 952(m), 823(s), 727(w), 691(w), 656(w), 536(s), 506(m) (Figure S7, Supplementary Part).

Catalytic oxidation of Cyclohexene

To a solution of cyclohexene (4 mmol), tert-butyl hydroperoxide (12 mmol) and 1,2,4-trichlorobenzene (4 mmol) (used as internal standard) in CH_2Cl_2 (5.0 mL) was added **1** (0.056 mmol based on cobalt) at room temperature. The reaction mixture was stirred at 80 °C in a closed heating tube. Aliquots of ca. 50 μL were taken after time steps indicated in Figure 8. Each sample was diluted with 1 mL CH_2Cl_2 and filtered through a 0.25 μm Acrodisc nylon filter. Then, the sample was analyzed by gas chromatography. For investigations on catalyst activities in subsequent multiple runs, the catalysts were separated from the reaction mixture by centrifugation and rinsed twice with dichloromethane before use.

X-ray Crystallography

Comparative examination of several crystal specimen revealed that crystals of compound **1** show a high tendency for crystal twinning.

Table 1 Single-crystal data and refinement summary for **1**.

Empirical formula	$C_{42}H_{58}N_{14}O_6Co_2$
Formula weight	972.88
T/K	100(2)
λ/Å	0.71073
Crystal system	monoclinic
Space group	$P2_1/c$
a/Å	13.327(3)
b/Å	14.151(3)
c/Å	26.532(6)
β/°	101.512(7)
V/Å^3	4903.0(19)
Z	4
D_{calcd} (Mg/m^3)	1.318
μ/mm^{-1}	0.735
F(000)	2040
θ range/°	1.56 to 26.43
Measured Reflections	11470
Independent Reflections	11470
Data/restraints/parameters	11470 / 463 / 590
R_1 [$I>2\sigma(I)$][a]	0.1339
wR_2 [$I>2\sigma(I)$][a]	0.3432
R_1 (all data)[a]	0.1607
wR_2 (all data)[a]	0.3592
Goodness-of-fit on F^2	1.112
$\Delta\rho_{max,\,min}$ /e·Å^{-3}	1.989 and −1.901

[a] $R_1 = \Sigma||F_o| - |F_c||/\Sigma|F_o|$. $wR_2 = \{\Sigma[w(F_o^2 - F_c^2)^2]/\Sigma[w(F_o^2)^2]\}^{1/2}$.

Crystal structure determination by X-ray diffraction was performed at 100 K on a Bruker APEX DUO diffractometer employing monochromatic Mo-Kα radiation (λ = 0.71073 Å). The twin cells were determined with Cell now (Sheldrick). Integration was done using SAINT simultaneously for two domains. Scaling and absorption correction was done using TWINABS resulting in HKLF4 and HKLF5 data. The initial structure was solved by direct methods from the HKLF4 data and refined against the HKLF5 data by full-matrix least squares techniques based on F^2 using the SHELXL-97 program [12]. (Information on the twinning domains: Rotation angle: 180°; Rotation vector (laboratory): −0.9494 0.0669 0.3068; Rotation vector (reciprocal cell): −0.00 0.00 −1.00, Rotation vector (direct cell): −2.00 0.00 −5.00; Unit cell relationships: a′ = −1 * a, b′ = +1 * b, c′ = −1 * c; Superposition matrix: H′ = −1.0 * H, K′ = −1.0 * K, L′ = +0.8 * H +1.0 * L; Domain ratios: 50 % / 50 %)

All non-hydrogen atoms were refined anisotropically. Hydrogen atoms were placed at calculated positions and refined using a riding model. The final residuals (R_1 = 0.1339, wR_2 = 0.3592) are relatively large, which is due to the relatively small size of crystal specimen obtained in solvothermal synthesis (< 80 μm), and to the rapid changes of lattice parameters upon loss of occluded solvent molecules in **1**. Depending on the stage of crystal aging, crystallographic parameters of **1** vary significantly, which is also reported in structurally similar compound MIL-53 [13]. Details of data collection and refinement of the compounds are summarized in Table 1. Selected bond distances and angles are given in Table 2.

Crystallographic data for the structure(s) have been deposited with the Cambridge Crystallographic Data Centre with No. CCDC 683431. Copies of the data can be obtained free of charge on application to The Director, CCDC, 12 Union Road, Cambridge CB2 1EZ, UK (Fax: int.code +(1223)336-033; e-mail for inquiry: fileserv@ccdc.cam.ac.uk; e-mail for deposition: deposit@ccdc.cam.ac.uk).

Table 2 Selected bond lengths /Å and angles /° of **1**.

Co(1)−N(6)	1.957(10)	Co(2)−N(5)	1.953(10)
Co(1)−N(1)	2.000(10)	Co(2)−N(2)	1.989(9)
Co(1)−N(3)	1.937(10)	Co(2)−N(8)	2.023(9)
Co(1)−N(7)	2.014(10)	Co(2)−N(4)	1.982(9)
N(3)−Co(1)−N(6)	101.7(4)	N(5)−Co(2)−N(4)	116.2(4)
N(3)−Co(1)−N(1)	111.2(4)	N(5)−Co(2)−N(2)	105.3(4)
N(6)−Co(1)−N(1)	120.1(4)	N(4)−Co(2)−N(2)	110.1(4)
N(3)−Co(1)−N(7)	108.5(4)	N(5)−Co(2)−N(8)	109.9(4)
N(6)−Co(1)−N(7)	108.2(4)	N(4)−Co(2)−N(8)	106.4(4)
N(1)−Co(1)−N(7)	106.7(4)	N(2)−Co(2)−N(8)	108.7(4)

Results and Discussion

Crystal Structure

X-ray crystallographic analysis reveals that **1** crystallizes in the monoclinic space group $P2_1/c$. The framework of **1** is constructed by cross-linking infinite 1D chains of Co^{II} ions, running in parallel at the crystallographic b direction, with anionic BPB^{2-} ligands. The structure of the 1D cobalt coordination chains in **1** is similar to the structure of [Co(pz)$_2$] described in ref. [9]. In the structure of **1**, each Co^{II} atom is placed in a tetrahedral coordination environment provided by four N-donor atoms which stem from different BPB^{2-} ligands, as shown in Figure 1. The Co^{II} atoms are bridged by adjacent BPB^{2-} ligands to form 6-membered {Co$_2$N$_4$} rings with a Co···Co distance of 3.55 Å. The 1D chains of Co^{II} atoms are cross-linked by linear tetradentate BPB^{2-} ligands that point towards crystallographic a and c directions, respectively, thus generating a 3D porous framework. Figure 2 displays a packing diagram of **1** with a single rectangular channel (approx. dim. 10.1 Å × 5.5 Å) running along the a axis of the crystal lattice.

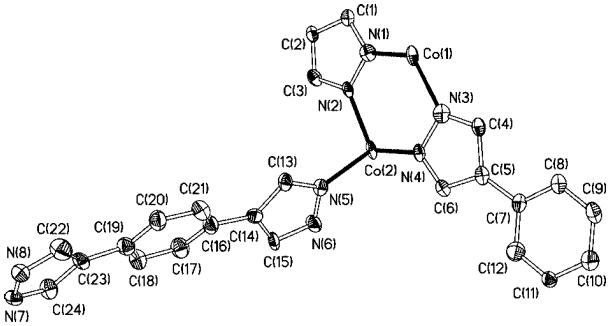

Figure 1 View of the asymmetric unit in **1**. All hydrogen atoms and DMF molecules have been omitted for clarity.

Thermal Stability

The study of thermal stability of **1** has been carried out by combining thermogravimetry (TG) analysis and variable-temperature X-ray powder diffraction (VTXRD). The TG analysis (Figure 3 and Table 3) of **1** shows that occluded DMF molecules are released up to a maximum temperature of 220 °C, yielding the desolvated MOF; no further weight loss occurs below 290 °C. The network of **1** decomposes in

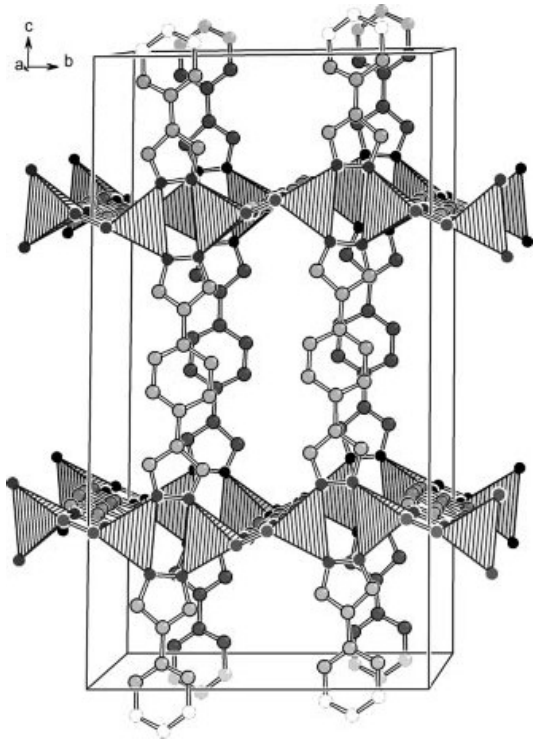

Figure 2 Crystal packing diagram of **1**. $\{CoN_4\}$ coordination units are represented as hatched polyhedrons. Occluded DMF molecules and hydrogen atoms are omitted for clarity.

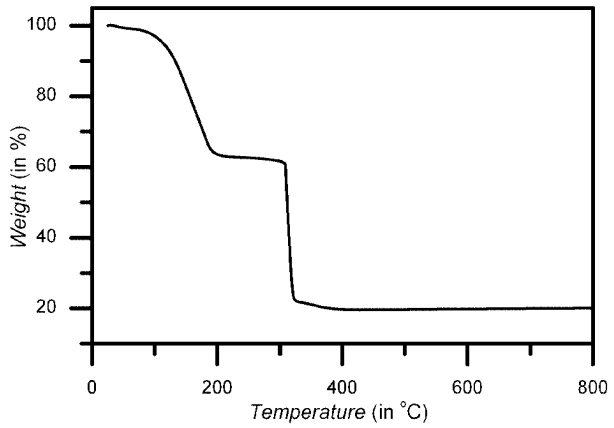

Figure 3 TG analysis curve of **1**.

Table 3 Observed weight loss for **1**.

Temperature	30–200 °C	290–390 °C
Observed weight loss	37 %	43 %
Calculated Weight loss	45 % [a]	38 % [b]

[a] calculated for $[Co^{II}(BPB)]\cdot 3DMF \rightarrow [Co^{II}(BPB)]$
[b] calculated for $[Co^{II}(BPB)] \rightarrow Co_3O_4$

the temperature range of 290 − 390 °C. The VTXRD patterns (Figure 4) suggest that the framework of **1** is stable up to 260 °C. Differences between the XRD patterns recorded in the temperature range between 30 and 250 °C are due to changes of crystallographic parameters upon removal of the solvent. The pore size distribution of **1** and its porosity characteristics obtained from argon sorption experiments indicate that the main structural features are still retained after heating at 150 °C for 30 h in vacuum. Moreover, when the sample is reimmersed in DMF after thermal treatment, the crystal structure is retained according to XRPD measurements (Figure 5). In addition, the UV/Vis diffuse reflectance spectra of **1** show only slight differences between a sample before or after heating for 12 h at 150 °C (Figures S4b and S10, Supplementary Part). These results indicate that the framework of **1** is stable upon complete removal of solvent molecules.

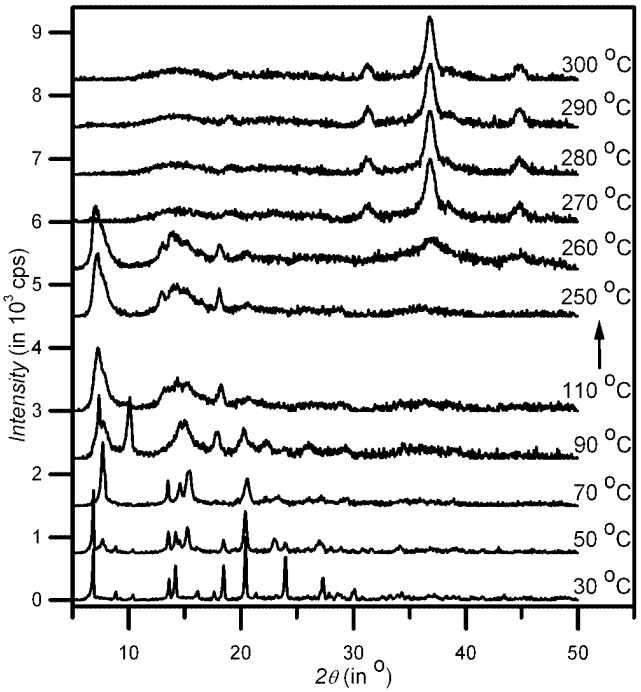

Figure 4 VTXRPD patterns of **1** in the range of 30–110 °C and 250–300 °C.

Porosity Characteristics

Compound **1** exhibits permanent porosity, which has been confirmed by argon gas sorption. After the catalytic reaction, the porosity of **1** is still retained. Prior to the measurement, the chloroform-exchanged samples were heated at 150 °C for 30 h under vacuum to remove any occluded solvent molecules. The isotherm of **1** obtained with argon gas sorption (Figure 6) reveals a type-IV sorption behavior, which is principally characteristic of solids with mesopores. The sorption behavior is changed to type-I after catalysis, typical for microporous material. The adsorption data were fitted to the BET equation to give a BET surface area of 1207 m^2/g for **1** (which is reduced to a value of 432 m^2/g after catalysis). The BET surface area for **1** is relatively high

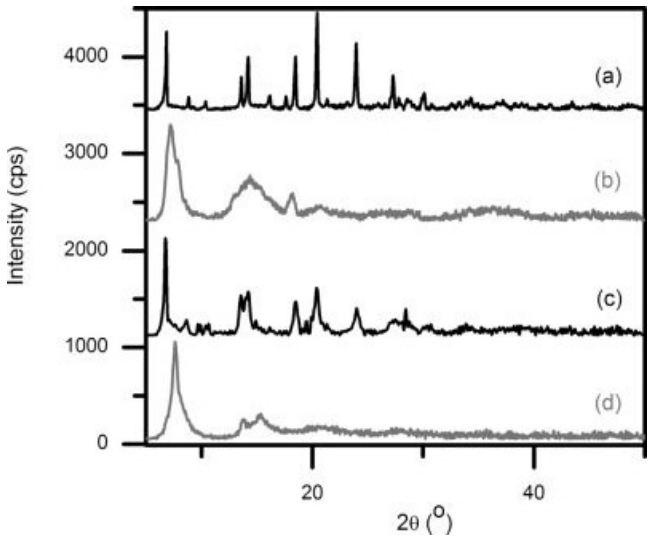

Figure 5 XRPD patterns for **1**. (a) before thermal treatment, (b) after thermal treatment for 30 h at 150 °C, (c) crystals reimmersed in DMF after thermal treatment, and (d) after catalysis.

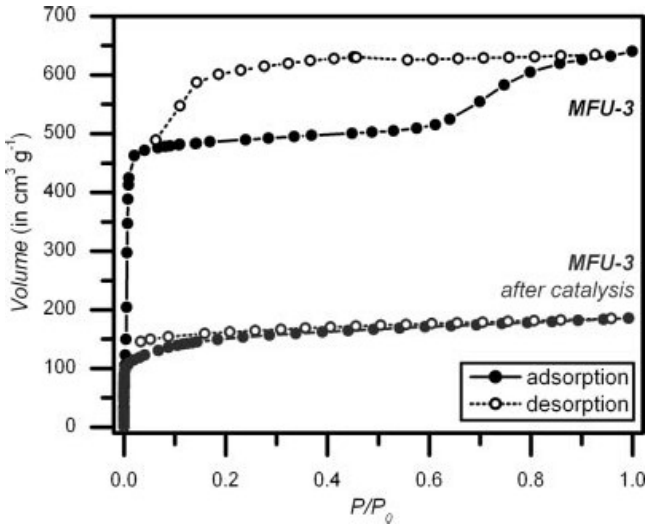

Figure 6 Argon adsorption isotherm at 77 K for a desolvated sample of **1**.

if compared to that of microporous zeolites and aluminophosphates, but lower than those of MOF-5 and its derivatives [14]. To evaluate the pore size distribution of **1**, the argon sorption isotherms measured at 77 K were analyzed using non-local density functional theory (NLDFT) [15] implementing a carbon equilibrium transition kernel for argon adsorption at 77 K based on a slit-pore model [16]. The distributions calculated by fitting the adsorption data indicate micropores with average dimensions of about 1.1 nm and, additionally, mesopores in the range of 4.5−7.0 nm (Figure 7). The diameter of the micropores is in good agreement with the average pore aperture calculated from the X-ray structure of **1** (1.0 nm based on vander-Waals radii). After catalysis, the pore diameter of 1 nm is still retained. We attribute the unexpected existence of mesopores to the flexibility (or breathing) of the network, since the observed adsorption behaviour is common for flexible framework structures [17].

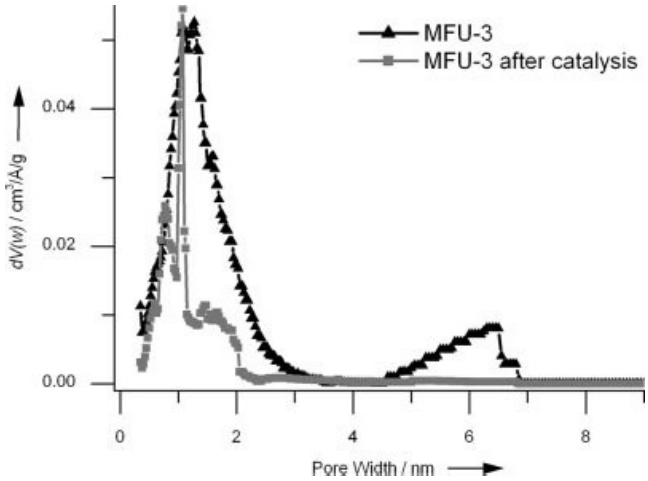

Figure 7 Pore size distributions for **1** before (black) and after catalysis (grey) calculated by fitting NLDFT models to the argon adsorption data.

UV/Vis Diffuse Reflectance Spectrum (DRS)

The UV/Vis diffuse reflectance spectrum of compound **1** (Figure S4, Supplementary Part) shows several absorption bands in the UV region, which correspond to intraligand $n \rightarrow \pi^*$ and $\pi \rightarrow \pi^*$ transitions. In the visible region, **1** exhibits a broad absorption band centered at 570 nm (17544 cm^{-1}), owing to the spin-forbidden d-d transitions of Co^{II} ions, which are in good agreement with literature values of tetrahedral Co^{II} complexes [18].

Catalytic Oxidation of Cyclohexene

As a test reaction for catalytic activity of **1**, the oxidation of cyclohexene was examined employing tert-butyl hydroperoxide as oxidant. In contrast to numerous reports on the (catalytic) oxidation of cyclohexane by Co^{II} complexes [6], the corresponding transformation of cyclohexene has been explored to a less extent [19]. The experimental data (Figure 8) demonstrate that oxidation of cyclohexene is fast and multiple turnover is achieved in the presence of **1**, (catalyst suspension in CH_2Cl_2, 80 °C, molar ratio of tert-butyl hydroperoxide / cyclohexene / cobalt centres = 214 / 71 / 1), whereas no reaction occurs in the absence of catalyst under the same conditions. The maximum substrate conversion achieved after 12 h was 62 %. The main reaction products are tert-butyl-2-cyclohexenyl-1-peroxide, 2-cyclohexe-1-one and cyclohexene oxide, as revealed by combined gas chromatographic and mass spectroscopic product analysis. **1** exhibits an exceptionally high selectivity toward allylic substitution, i.e. formation of tert-butyl-2-cyclohexenyl-1-peroxide (ca. 83 %). A similar catalytic substrate conversion

for the oxidation of cyclohexene was recently achieved by immobilization of low-molecular cobalt complexes to alumina supports [20]. During catalysis crystals of **1** undergo structural changes, leading to broad reflexes in the XRPD (Figure 5d). BET results show that the specific surface of **1** is reduced and that the desorption hysteresis disappears, but nevertheless the compound is still porous (Figure 6). Additionally, the pore size distribution reveals that the mesopores (above 4 nm) disappear and that micropores of 1 nm diameter are still observed (Figure 7). This clearly indicates that the porous structure of **1** is retained, since the open channels in **1** have an average pore aperture of 1.0 nm (as calculated from the X-ray structural data). We ascribe the changes in pore size distribution to the "breathing" of the flexible network. The unit cell metrics of **1** display dynamic changes during the course of catalysis, but the porous network structure stays intact.

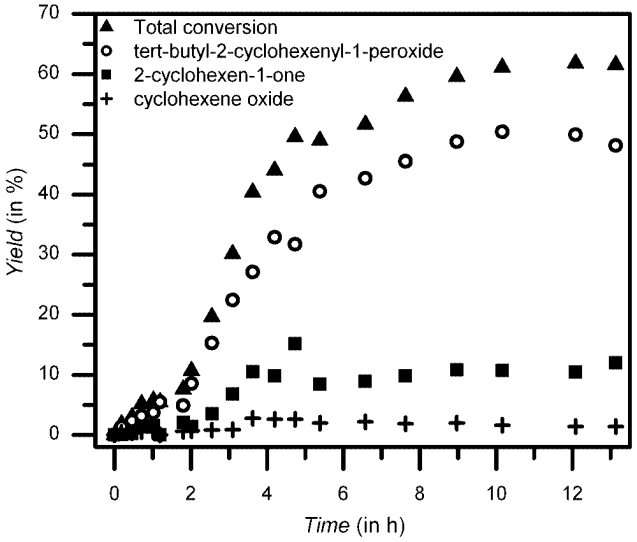

Figure 8 Yield (%) vs time (h) curves for cyclohexene oxidation with **1** as catalyst.

In summary, we have prepared a novel MOF, which contains redox-active Co^{II} atoms. **1** possesses a 3D porous framework which is built up by cross-linking 1D chains of Co^{II} atoms with $(BPB)^{2-}$ ligands coordinating to the metal ions. The framework of **1** is stable upon complete removal of solvent molecules although some changes of lattice parameters occur and the crystals develop cracks and voids upon prolonged exposure to high-vacuum. Using **1** as catalyst, the oxidation reaction of cyclohexene is fast and multiple turnover is achieved (Figure S9, Supplementary Part). The experimental results demonstrate that catalytic oxidation reactions employing redox-active MOFs are principally feasible and future developments in this direction should be rewarding.

Acknowledgements. The authors thank BRUKER AXS (Leo Straver, Delft) for providing X-ray data for compound **1**, and for help and fruitful discussions on conducting the twinning refinements. Financial Support by DFG (Priority Program SPP 1362 "Porous Metalorganic Frameworks") is gratefully acknowledged.

References

[1] a) X. Zhao, B. Xiao, A. J. Fletcher, K. M. Thomas, D. Bradshaw, M. J. Rosseinsky, *Science* **2004**, *306*, 1012–1015; b) H. G. Schimmel, G. J. Kearley, M. G. Nijkamp, C. T. Visser, K. P. de Jong, F. M. Mulder, *Chem. Eur. J.* **2003**, *9*, 4764–4770; c) E. Brunet, H. M. H. Alhendawi, C. Cerro, M. J. de la Mata, O. Juanes, J. C. Rodríguez-Ubis, *Angew. Chem.* **2006**, *118*, 7072–7074; *Angew. Chem. Int. Ed.* **2006**, *45*, 6918–6920; d) J. S. Seo, D. Whang, H. Lee, S. I. Jun, J. Oh, Y. J. Jeon, K. Kim, *Nature* **2000**, *404*, 982–986; e) P. Feng, X. Bu, G. D. Stucky, *Nature* **1997**, *388*, 735–741.

[2] a) L. Schlapbach, A. Züttel, *Nature* **2001**, *414*, 353–358; b) J. L. C. Rowsell, O. M. Yaghi, *Angew. Chem.* **2005**, *117*, 4748–4758; *Angew. Chem. Int. Ed.* **2005**, *44*, 4670–4679.

[3] a) C. Livage, N. Guillou, J. Chaigneau, P. Rabu, M. Drillon, G. Férey, *Angew. Chem.* **2005**, *117*, 6646–6649; *Angew. Chem. Int. Ed.* **2005**, *44*, 6488–6491; b) S. M. Humphrey, J. Chang, S. H. Jhung, J. W. Yoon, P. T. Wood, *Angew. Chem.* **2007**, *119*, 276–279; *Angew. Chem. Int. Ed.* **2007**, *46*, 272–275; c) M. Dincă, A. F. Yu, J. R. Long, *J. Am. Chem. Soc.* **2006**, *128*, 8904–8913; d) N. L. Rosi, J. Kim, M. Eddaoudi, B. Chen, M. O'Keeffe, O. M. Yaghi, *J. Am. Chem. Soc.* **2005**, *127*, 1504–1518; e) C. Wu, W. Lin, *Angew. Chem.* **2005**, *117*, 1994–1997; *Angew. Chem. Int. Ed.* **2005**, *44*, 1958–1961.

[4] a) L. Alaerts, E. Séguin, H. Poelman, F. Thibault-Starzyk, P. A. Jacobs, D. E. De Vos, *Chem. Eur. J.* **2006**, *12*, 7353–7363; b) S.-H. Cho, B. Ma, S. T. Nguyen, J. T. Hupp, T. E. Albrecht-Schmitt, *Chem. Commun.* **2006**, 2563–2565; c) S. Hasegawa, S. Horike, R. Matsuda, S. Furukawa, K. Mochizuki, Y. Kinoshita, S. Kitagawa, *J. Am. Chem. Soc.* **2007**, *129*, 2607–2614; d) R.-Q. Zou, H. Sakurai, S. Han, R.-Q. Zhong, Q. Xu, *J. Am. Chem. Soc.* **2007**, *129*, 8402–8403; e) C.-D. Wu, W. Lin, *Angew. Chem.* **2007**, *119*, 1093–1096; *Angew. Chem. Int. Ed.* **2007**, *46*, 1075–1078.

[5] Y. Lu, M. Tonigold, B. Bredenkötter, D. Volkmer, B. Rieger, S. Bahnmüller, J. Hitzbleck, G. Langstein, *submitted*.

[6] a) F. A. Chavez, J. M. Rowland, M. M. Olmstead, P. K. Mascharak, *J. Am. Chem. Soc.* **1998**, *120*, 9015–9027; b) F. A. Chavez, J. A. Briones, M. M. Olmstead, P. K. Mascharak, *Inorg. Chem.* **1999**, *38*, 1603–1608; c) L. Saussine, E. Brazi, A. Robine, H. Mimoun, J. Fischer, R. Weiss, *J. Am. Chem. Soc.* **1985**, *107*, 3534–3540; d) D. K. Chand, P. K. Bharadwaj, *Inorg. Chem.* **1997**, *36*, 5658–5660.

[7] a) P. Feng, X. Bu, S. H. Tolbert, G. D. Stucky, *J. Am. Chem. Soc.* **1997**, *119*, 2497–2504; b) J. M. Thomas, R. Raja, G. Sankar, R. G. Bell, *Nature* **1999**, *398*, 227–230.

[8] S. Ma, H.-C. Zhou, *J. Am. Chem. Soc.* **2006**, *128*, 11734–11735.

[9] N. Masciocchi, G. A. Ardizzoia, S. Brenna, G. LaMonica, A. Maspero, S. Galli, A. Sironi, *Inorg. Chem.* **2002**, *41*, 6080–6089.

[10] a) STERLING DRUG INC (US) (D. M. Bailey, V. Kumar), U.S. 4888352 (December 19, 1989); b) V. Lozan, P. Y. Solntsev, G. Leibeling, K. V. Domasevitch, B. Kersting, *Eur. J. Inorg. Chem.* **2007**, 3217–3226.

[11] M. A. Warpehoski, B. Chabaud, K. B. Sharpless, *J. Org. Chem.* **1982**, *47*, 2897–2900.

[12] G. M. Sheldrick, *SHELXL-97*, *Program for X-ray Crystal Structure Refinement*, University of Göttingen, Göttingen, Germany, 1997.

[13] C. Serre, F. Millange, C. Thouvenot, M. Noguès, G. Marsolier, D. Louër, G. Férey, *J. Am. Chem. Soc.* **2002**, *124*, 13519–1352.

[14] a) H. Li, M. Eddaoudi, M. O'Keeffe, O. M. Yaghi, *Nature* **1999**, *402*, 276−279; b) M. Eddaoudi, J. Kim, N. Rosi, D. Vodak, J. Wachter, M. O'Keeffe, O. M. Yaghi, *Science* **2002**, *295*, 469−472.

[15] a) P. I. Ravikovitch an A. V. Neimark, *Colloids and Surfaces* **2001**, *187*−*188*, 11−21; b) S. J. Gregg, K. S. W. Sing, *Adsorption, Surface Area and Porosity*, 2nd.ed., Academic Press, London 1982, p. 42.

[16] J. Jagiello, M. Thommes, *Carbon* **2004**, *42*, 1227−1232.

[17] a) E. J. Cussen, J. B. Claridge, M. J. Rosseinsky, C. J. Kepert, *J. Am. Chem. Soc.* **2002**, *124*, 9574−9581; b) T. K. Maji, G. Mostafa, R. Matsuda, S. Kitagawa, *J. Am. Chem. Soc.* **2005**, *127*, 17152−17153; c) P. L. Llewellyn, S. Bourrelly, C. Serre, Y. Filinchuk, G. Férey, *Angew. Chem., Int. Ed.* **2006**, *45*, 7751−7754; d) A. Kondo, H. Noguchi, L. Carlucci, D. M. Proserpio, G. Ciani, H. Kajiro, T. Ohba, H. Kanoh, K. Kaneko, *J. Am. Chem. Soc.* **2007**, *129*, 12362−12363; e) C. Serre, C. Mellot-Draznieks, S. Surblé, N. Audebrand, Y. Filinchuk, G. Férey, *Science* **2007**, *315*, 1828−1831.

[18] a) A. B. P. Lever, in *Inorganic Electronic Spectroscopy*, Elsevier Publishing Company, Amsterdam, 1968, Ch. 9, p. 323; b) L. Poul, N. Jouini, F. Fiévet, *Chem. Mater.* **2000**, *12*, 3123−3132.

[19] a) J. D. Koola, J. K. Kochi, *J. Org. Chem.* **1987**, *52*, 4545−4553. b) M. S. Kharasch, A. Fono, *J. Org. Chem.* **1959**, *24*, 72−78.

[20] M. Salavati-Niasari, M. Hassani-Kabutarkhani, F. Davar, *Catal. Commun.* **2006**, *7*, 955−962.